11th International Conference on Green Energy & Environmental Engineering (GEEE-2025)
Proceedings of Engineering & Technology – PET-Vol 94, pp.88-93

Reliable Measurement of electron Diffusion Coefficient Using the (EPE) Technique: Insights into n-type GaAs-based detectors.

M.A. Soussou[#1], I. Mellouki[#2], N. Khaldi[#3] and M. Lazaar[#4]

[#]Thermal Process Laboratory, Research and Technology Centre of Energy, Borj-Cedria Science and Technology Park, B.P. 95, 2050 Hammam-Lif, Tunisia.
[1]mohamedakram.soussou@gmail.com
[2]imene.mellouki@ipeit.rnu.tn
[3]khaldi.nawel@yahoo.fr
[4]mariem.lazaar@crten.rnrt.tn

***Abstract*— This study investigates the electron diffusion coefficient in n-type GaAs with a low carrier concentration of $Nd=10^{21}m^{-3}$ using the ElectroPyroElectric (EPE) technique. This non-destructive and cost-effective method is enhanced through a normalization procedure within our theoretical framework. Compared to conventional Electrochemical Impedance Spectroscopy (EIS), the EPE technique demonstrates superior reliability and consistensy in measuring Electronic transport parameters. Through a comprehensive experimental analysis of the Nyquist diagram over a frequency range from 1 Hz to 100 kHz and modeling via the Randles equivalent circuit, we determine a diffusion coefficient of $D=1.02\times10^{-4}$ m^2s^{-1}. This corresponds to a diffusion time response of around 0.1 ms, indicating relatively fast carrier dynamics. Although this value is lower than those reported in existing literature, the discrepancy is primarily attributed to boundary effects and assumptions inherent in the semi-infinite Warburg model. Future work will involve fitting the experimental impedance to an Open-Warburg model, which better reflects the physical configuration and allows for more accurate diffusion coefficient estimation.**

***Keywords*—EPE Technique, n-type GaAs, Nyquist diagram, Warburg impedance, electron diffusion coefficient.**

I. INTRODUCTION

Recent advancements in understanding charge carrier transport have emphasized its critical role in enhancing the performance of GaAs-based detectors, particularly under high-energy irradiation [1]. Among semiconductor materials, n-type GaAs (Gallium Arsenide with n-type dopants) is distinguished by its high electron mobility, making it a strong candidate for applications in radiation detection and advanced energy devices [2,3]. Due to différences in doping and carrier mobility, n-type GaAs typically exhibit a higher electronic diffusion coefficient than its p-type counterpart [4]. The diffusion coefficient—a key factor for semiconductor performance—can be assessed using Electrochemical Impedance Spectroscopy (EIS) by examining the Warburg impedance in the low-frequency domain of the Randles circuit [5]. Although effective, EIS does not provide unique results for every material [6]. Variations in material characteristics can significantly alter impedance behaviors, thus affecting the Nyquist plot shape [7]. To overcome these limitations, the ElectroPyroElectric (EPE) method offers a robust theoretical framework for calculating semiconductor electrical impedance [8,9]. Unlike traditional techniques, EPE accounts for sample-specific attributes such as thermal properties and thickness, enabling a more tailored analysis. This study chose a thick n-type GaAs sample due to its low dopant density to analyze the uniqueness of its Nyquist diagram across a frequency range of 1 Hz to 100 kHz using the EPE methodology. The diffusion coefficient was also measured to examine the technique's applicability in advanced detector systems and related fields.

II. EPE THEORY

The pyroelectric (PE) detector features a 25 μm thick polyvinylidene fluoride (PVDF) layer. A 125μm

ISSN: 1737-9334

Mylar film is meticulously placed on the PVDF sensor to prevent short-circuiting. The sample(s) under examination, pressed mechanically against the pyroelectric cell, consists of an n-type GaAs with a thickness of 440µm and a doping density of $N_d = 10^{21}$ m^{-3}, elaborated by Molecular Beam Epitaxy [10] and has a thermal diffusivity of D_s=3.1×10^{-7}m²/s [11]. The depletion width is approximately 1.77µm, maintained to support electron diffusion. A 6 mm-thick copper substrate underpins the entire assembly, ensuring strong thermal contact and quickly enabling the pyroelectric signal to reach thermal equilibrium. The 1D model used in EPE theory under a temperature field produced by a periodic electrical excitation ($\omega=2\pi f$) through an alternating current (AC) is validated in [12]. Measurements were conducted across frequencies from 1 Hz to 100 kHz using a pulse generator and two copper electrodes set 1 cm apart , with a circular contact area $A=2\pi.10^{-6}$m². Instrumental effects were minimized through a normalization procedure using an empty sensor (without the GaAs sample), allowing for the isolation of the sample's contribution. The normalized configurations of the PE detector incorporated up to four layers (i), (i, m=Mylar, p=PVDF, b=substrate in copper), as depicted in Fig.1(a, b). The 1D complex thermal wave vector is $\sigma_i = \frac{1+j}{\mu_i}$, with $\mu_i = \sqrt{\frac{D_i}{\pi \cdot f}}$ being the thermal diffusion length in the material (i). To simplify the model, extreme values of thermal transport coefficients were used to match the specific sensor design. The intricated electrical impedance, Z_s, is defined as the ratio of the average pyroelectric voltage $< V_p(\omega) >$ across the sample to the pyroelectric voltage $< V_{sensor}(\omega) >$ of the empty sensor as described by the following equation: $Z_s(\omega) = \frac{< V_p(\omega) >}{< V_{sensor}(\omega) >} \cdot \Gamma_i(\omega) \cdot Z_{sensor}(\omega)$; where $\Gamma_i(\omega)$ is a function dependent of σ_i, the thermal conductivity and the thickness of material (i); and Z_{sensor} (ω) is the electrical impedance of the empty sensor, measured by an impedance meter in operating frequency ranges [13]. Further, the electrical impedance Z_s of n-type GaAs at frequency f, is defined as: $Z_s(\omega) = Z' + jZ''$, where Z' is the real and Z'' is the imaginary parts of Z_s.

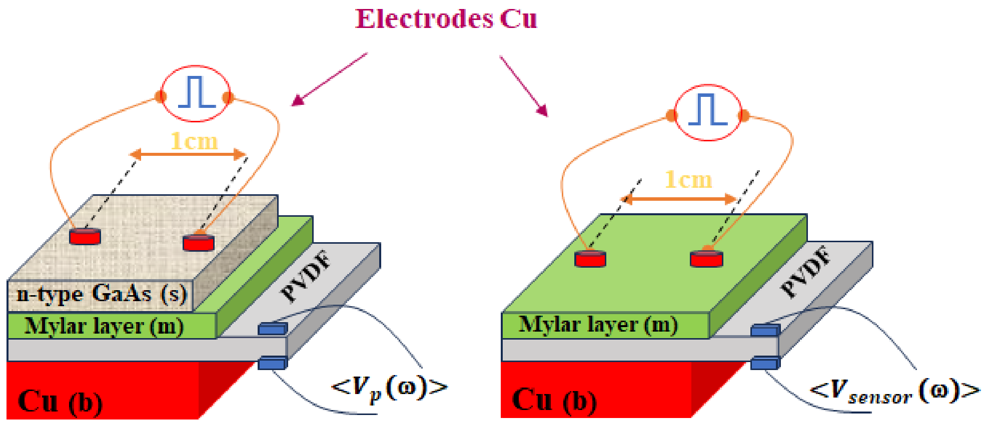

(a) (b)

Fig.1 Schematic diagram showing a perspective view of the Normalization Procedure used in EPE Theory
(a) The pyroelectric detector within the n-type GaAs. (b) The empty sensor.

III. EXPERIMENTAL SET-UP

Details of the EPE technique setup are provide in [12,13]. Fig. 2 illustrates the block diagram of the measurement system, which includes the PE cell placed within a grounded metallic enclosure acting as a Faraday cage. Modulated heating is applied using a pulsed voltage (V_a=1 V) from a generator operating over the 1 Hz -100 kHz range. The EPE signals, encompassing both amplitude and phase, are measured across the PVDF electrodes for each configuration. These signals are convertef from current to voltage, amplified, and

ISSN: 1737-9334

analyzed using a lock-in amplifier. Final data processing was performed using Maple 12.0 and Microcal Origin 9.0.

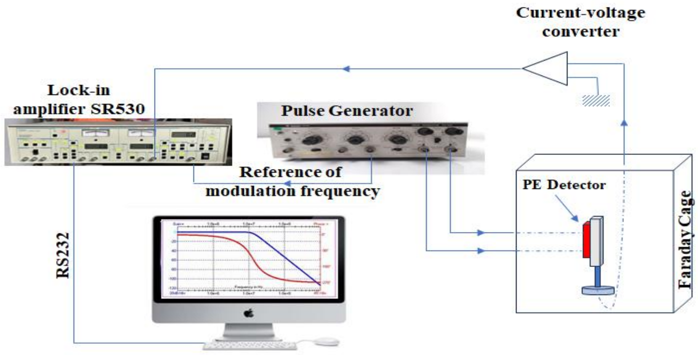

Fig.2 Diagram of the EPE Technique Setup

IV. RESULTS AND DISCUSSIONS

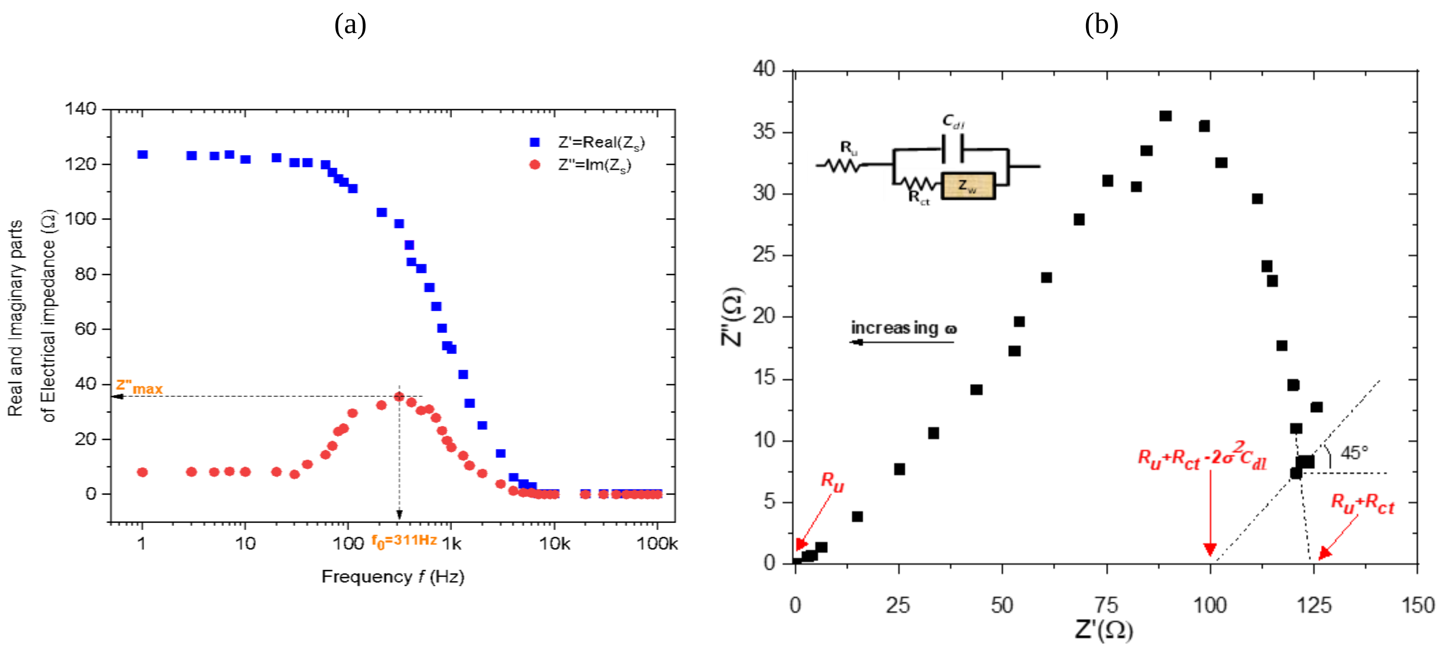

Fig.3: (a) The real Z' and the imaginary part Z" of electrical impedance Z_s according to the frequencies. (b) The Nyquist Diagram and the Randles equivalent circuit of n-type GaAs by the EPE technique.

Fig. 3(a) displays the sample's impedance spectrum. At low frequencies, the real part of the impedance (Z′) is dominant, reflecting resistive behavior. As the frequency rises, the real part of Z_s decreases because charge carriers become less responsive to the alternating electric field, resulting in fewer scattering events and reduced resistance. When the frequency exceeds approximately 7 kHz, the material shifts to purely capacitive behavior, with its response mainly determined by its ability to store charge carriers that can no longer keep up with the high-frequency alternating signal. This transition allows more current to flow while dielectric polarization effects lessen, as they cannot match the rapid oscillations. Fig. 3 (b) shows the Nyquist diagram of n-type GaAs (Z" versus Z' on a complex plane), depicting a semicircular arc at high frequencies transotioning to a linear tail at lower frequencies. The asymmetry of the semicircle is, suggests parasitic inductance at high frequencies, reflecting magnetic fields produced by currents in the contact or

ISSN: 1737-9334

semiconductor. The Randles equivalent circuit for n-type GaAs, illustrated in the top-left corner of Fig. 3 (b), features a series resistance R_u that represents the total resistance to charge flow. This includes contributions from the GaAs material, the Cu-GaAs contact resistance, and the resistance of the pyroelectric detector, which is connected in parallel with the double-layer capacitance C_{dl}. This capacitance corresponds to the charge separation at the GaAs/Cu interface, influenced by the electron density in the semiconductor.

The circuit also features Faradic impedance, which comprises charge transfer resistance (R_{ct}). This resistance indicates the challenges related to charge injection or extraction between the GaAs and copper electrodes, influenced by interface quality and the Schottky barrier at the Cu-GaAs junction. This is in series with Warburg impedance (Z_w), representing the difficulties in electron mass transport to the electrode [14]. The values found from Nyquist Diagram are R_u =0.7Ω and R_{ct}=125.5 Ω. The imaginary part of the impedance, due to the capacitance C_{dl}, receives its maximum value Z''_{max} at the frequency f_0 (f_0=311Hz), where $C_{dl} = \frac{1}{2\pi f_0 R_{ct}}$ = 4.1μF. In the low-frequency range, the real part Z' can be extrapolated to cross the real axis (x-axis) at $Z'=R_u+R_{ct}-2\sigma^2C_{dl}$, where σ is the Warburg coefficient [7], with our estimated value of $1.86.10^3\Omega.s^{-1/2}$. Using the semi-infinite Warburg model, the electronic diffusion coefficient D of n-type GaAs, can be modelled across the GaAs/Cu interface using the Warburg coefficient σ as: $\sigma = \frac{RT}{n^2F^2CA\sqrt{2D}}$, where R is the gas constant ($8.314J.mol^{-1}K^{-1}$), n is number of the transferred electrons (n=1), F is the Faraday's constant ($96485C.mol^{-1}$), T is the temperature (300K), C is the concentration of dopant ($0.16.10^{-2}mol.m^{-3}$) while $A=2\pi.10^{-6}m^2$. This experiment yields a diffusion coefficient of D=1.02×cm²s^{-1} which gives a response diffusion time $\tau_D = \frac{l_s^2}{\pi^2 D}$ to be 0.163ms. This value is significantly lower than the expected literature value (D~4.3 cm²/s for a doping concentration of around 10^{18} m^{-3}) [15,16]. Several factors explain this discrepancy: Given that the diffusion coefficient relates inversely to doping concentration as depositing at exceedingly low densities often results in impurities, increased defects, and inhomogeneities during sample synthesis. However, the main reason for the discrepancy lies in the semi-infinite Warburg model's assumptions, which are not valid for our setup, since the Mylar film introduces a blocking (reflective) boundary condition that limits diffusion across the bottom interface. The model assumes perfect or infinite diffusion domains, ignoring the reflective nature of the Mylar boundary. To address this, we propose adopting the finite-length (open) Warburg model [17], which accommodates real boundary conditions $Z_W = R_W \cdot (\frac{1}{\sqrt{j\omega\tau_D}}) \cdot \tanh(\sqrt{j\omega\tau_D})$; where R_W is the limiting diffusion resistance, related to carrier concentration and mobility. This model transitions smoothly from diffusion-dominated to capacitive behavior. For practical impedance fitting, it is often approximated by a parallel network $R_W||C_W$.

While a preliminary diffusion value was extracted, a complete fitting of the experimental impedance data to the open Warburg model has not yet been performed. This task remains a priority and presents considerable complexity since accurate low-frequency measurements are needed, fitting must be performed using advanced tools (e.g., ZView), and nonlinear regression is required for reliable parameter extraction. Such a fit would allow a more precise determination of D, reflecting the true influence of mixed boundary conditions.

V. CONCLUSIONS

The EPE technique has been successfully applied to estimate the diffusion coefficient in low-doped n-type GaAs. A preliminary value was obtained using the semi-infinite Warburg model; however, discrepancies with literature values highlight the importance of boundary conditions and model selection. The reflective Mylar boundary limits diffusion and invalidates the assumptions of the semi-infinite model.

ISSN: 1737-9334

The Open-Warburg model, which better accounts for experimental geometry and boundary effects, represents a more suitable framework for extracting accurate diffusion parameters. Future work will involve full model fitting to validate the EPE technique's effectiveness in complex semiconductor systems.

REFERENCES

[1] Petr Smolyanskiy, Petr Burian, Mateusz Sitarz and Benedikt Bergmann. *Experimental Determination of the Charge Carrier Transport Models for Improving the Simulation of the HR GaAs:Cr Detectors' Response*. Sensors 2023, 23, 6886. https://doi.org/10.3390/s23156886

[2] Salehi, A., Naderi, P., Boroumand, F.A. et al. (1 more author) (2018) *Fabrication and characterization of hybrid photovoltaic devices based on N-type GaAs and polymer composites.* In: Proceedings of the 2nd International Conference of Energy Harvesting, Storage, and Transfer (EHST'18). 2nd International Conference on Energy Harvesting, Storage, and Transfer (EHST'18), 07-09 Jun 2018, Niagara Falls, Canada. International ASET Inc., pp. 116-1. ISBN 9781927877456.

[3] Fu, HC., Li, W., Yang, Y. et al. An efficient and stable solar flow battery enabled by a single-junction GaAs photoelectrode. *Nat Commun* **12**, 156 (2021). https://doi.org/10.1038/s41467-020-20287-w

[4] S. George, P. Suresh Kumar, P. Radhakrishnan, V.P.N. Nampoori, C.P.G. Vallabhan, Proc. SPIE-Int. Soc. Opt. Eng. (2002) 4918.

[5] Orazem, M. E.; Tribollet, B. A Tutorial on Electrochemical Impedance Spectroscopy. ChemTexts 2020, 6 (2), 12

[6] Magar HS, Hassan RYA, Mulchandani A. Basic Concept of EIS : Electrochemical Impedance Spectroscopy (EIS): Principles, Construction, and Biosensing Applications. Sensors (Basel). 2021 Oct 1;21(19):6578. doi: 10.3390/s21196578. PMID: 34640898; PMCID: PMC8512860.

[7] Alexandros Ch. Lazanas Mamas I. Prodromidis. Electrochemical Impedance Spectroscopy─A Tutorial, ACS Meas. Sci. Au 2023, 3, 3, 162–193.https://doi.org/10.1021/acsmeasuresciau.2c00070

[8] Mellouki, I. "Thermo-electrical properties of semiconductors by the new electro pyro electric technique." *Int. J. Eng. Sci. Innovative Technol* 3.3 (2014): 314-319.

[9] N Bennaji, I. Mellouki, N. Yacoubi, Electrical impedance spectroscopy of Si by Electro-PyroElectric (E.P.E.) technique, July 2018, Conference: Complex impedance diagram of Si by Electro-PyroElectric (E.P.E.) technique, NANOTECH Tunisia 2014 and MEET Tunisia 2014 joint International Conferences and Exhibitions

[10] S. Abroug, F. Saadallah, F. Genty, N. Yacoubi, Investigation of electrical and optothermal properties of Si-doped GaSb epitaxial layers by the Hall effect, PL measurement and photothermal deflection spectroscopy, Physics Procedia, Volume 2, Issue 3, 2009,Pages 787-795,https://doi.org/10.1016/j.phpro.2009.11.026.

[11] Thermal properties of Gallium Arsenide (GaAs),https://www.ioffe.ru/SVA/NSM/Semicond/GaAs/thermal.html#:~:text=Density%20of%20 Gallium%20 Arsenide

[12] I. Mellouki, A. Mami, N. Bennaji, Y. Fadhli. Study of doping and annealing effects on thermal properties of SnxSb2Sy (1≤ x≤ 3, 4≤ y≤ 6) sulfosalts thin films by electro-pyroelectric technique, Thermochimica Acta, Volume 670, 2018, Pages 123-127, https://doi.org/10.1016/j.tca.2018.10.021.

[13] A Mami, N Bennaji, I Mellouki, N Yacoubi, *A thermo-electrical parameter investigation using pyroelectric techniques: Application on Mylar*,International Journal of Polymer Analysis and Characterization 22 (2), 118-124(2016).

[14] Jun Huang, Diffusion impedance of electroactive materials, electrolytic solutions and porous electrodes: Warburg impedance and beyond, Electrochimica Acta, Volume 281, 2018, Pages 170-188, https://doi.org/10.1016/j.electacta.2018.05.136.

[15] P M Nikolic *et al.* Transport properties of carriers in GaAs obtained using the photoacoustic method with the transmission detection configuration.J. Phys.: Condens. Matter 8 (1996) 5673–5683.DOI 10.1088/0953-8984/8/30/016

[16] S. Ilahi, Doping effects on minority carrier parameters in bulk GaAs, Physica B: Condensed Matter, Volume 652, 2023, https://doi.org/10.1016/j.physb.2022.414612.

[17] Nguyen, T. Q., & Breitkopf, C. (2018). Determination of diffusion coefficients using impedance spectroscopy data. *Journal of The Electrochemical Society*, *165*(14), E826-E831.

ISSN: 1737-9334